

1 **RADIATIVE FORCING BY CO<sub>2</sub> OBSERVED AT**  
2 **TOP OF ATMOSPHERE FROM 2002-2019**

3 **C. P. Rentsch**

4 <sup>1</sup>Midland, MI, USA

5 **Key Points:**

- 6 • Global radiance measurements under nighttime, cloud-clear conditions reveal  $0.358 \pm 0.067$   
7  $\text{Wm}^{-2}$  of CO<sub>2</sub>-induced radiative forcing, or 70% of IPCC model predictions.

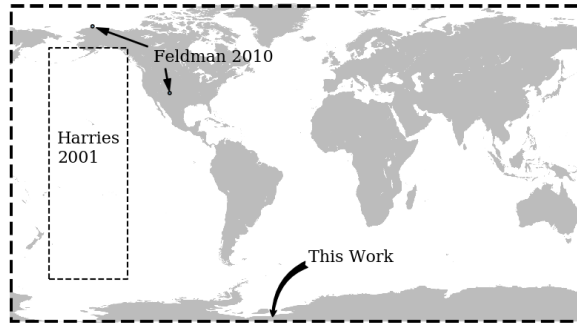


**Figure 1.** Measurement coverage for this work and select prior works by others

8

## Abstract

9

10

11

12

13

14

15

16

17

Spectroscopic measurements at top-of-atmosphere are uniquely capable of attributing changes in Earth’s outgoing infrared radiation field to specific greenhouse gasses. The Atmospheric Infrared Sounder (AIRS) placed in orbit in 2002 has spectroscopically resolved a portion of Earth’s outgoing longwave radiation for 17 years. Concurrently, atmospheric CO<sub>2</sub> rose from 373 to 410 ppm, or 28% of the total increase over pre-industrial levels. The IPCC Fifth Assessment Report predicted  $0.508 \pm 0.102 \text{ Wm}^{-2}$  additional radiative forcing from this CO<sub>2</sub> increase. Here it is shown that global measurements under nighttime, cloud-clear conditions reveal  $0.358 \pm 0.067 \text{ Wm}^{-2}$  of CO<sub>2</sub>-induced radiative forcing, or 70% of IPCC model predictions.

18

## Introduction

19

20

21

22

23

24

25

26

27

28

29

30

31

32

33

34

Increasing infrared absorption caused by rising CO<sub>2</sub> is the foundational physical mechanism underpinning the anthropogenic global warming hypothesis. Despite numerous studies on global temperature trends and rising greenhouse gas concentrations, very few investigations offer long term spectrophotometric measurement of CO<sub>2</sub> altering Earth’s outgoing longwave radiation (OLR). Harries et al. (2001) compared 529 OLR spectra measured by the IRIS satellite in 1970 to 4,061 spectra measured by IMG in 1996 over the Pacific Ocean. Feldman et al. (2015) reported increasing downwelling longwave radiation (DLR) in two 1.6° conical upward views of the atmosphere between 2000 and 2010 (figure 1). Neither study provides a global assessment of CO<sub>2</sub>-induced radiative forcing. The Atmospheric Infrared Spectrophotometer (AIRS) offers the longest record among all current or previous satellite spectrophotometers and has measured Earth’s OLR while atmospheric CO<sub>2</sub> concentration rose from 373 to 410 ppm, 28% of the total increase since 1750. This work examines 50.7 billion global nighttime, cloud-clear spectral radiance measurements (hereafter: radiances) made by AIRS during the last seventeen years. Figure 2 exemplifies a single OLR spectrum comprised of 2,378 radiances. AIRS does not have measurement capability at  $<649.6 \text{ cm}^{-1}$ ,  $1136\text{-}1217 \text{ cm}^{-1}$  or  $1614\text{-}2181 \text{ cm}^{-1}$ .

35

## 1 Data

36

37

38

39

40

41

The majority of satellite views of Earth contain clouds that reflect or absorb upwelling infrared (IR). Cloud-clear scenes are preferred to avoid attributing cloud-induced OLR reductions to CO<sub>2</sub>. The AIRS version 6 level 2 data product (Teixeira, 2013) quantifies fractional cloud content (*Tot.Cld4.CCfinal* field in *AIRS2CCF.006*) ranging from 0.00 to 1.00. This work utilizes radiances with 0.00 cloud fraction; only 11% of radiances meet this criterion. Although AIRS Level 2 measurements are a cloud-cleared data prod-

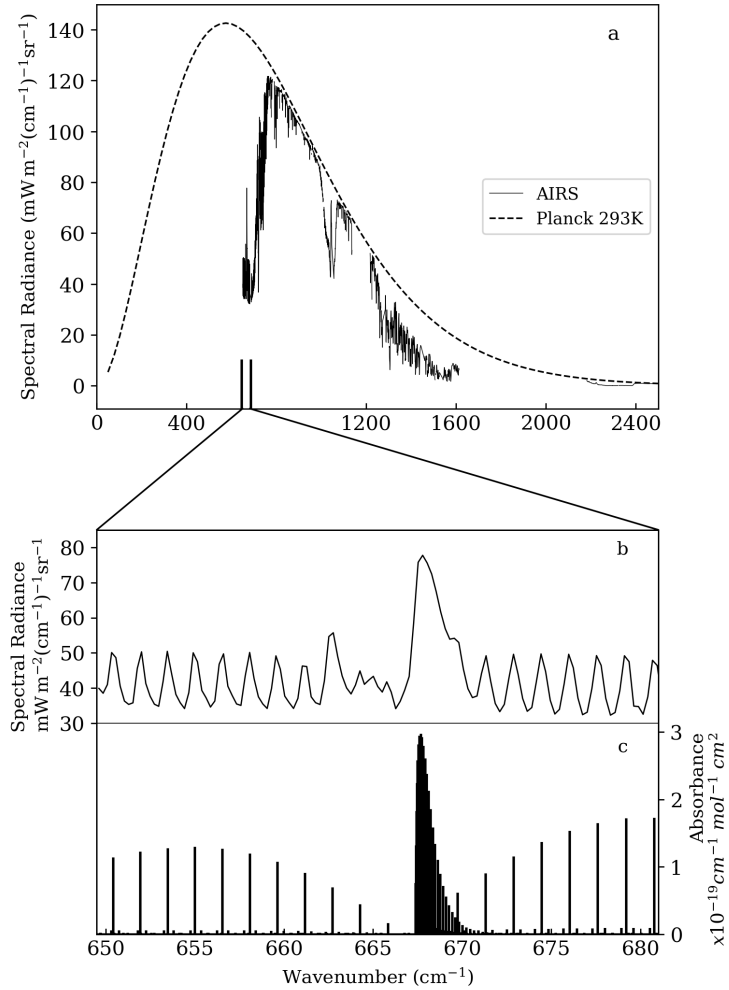


**Figure 2.** [a] AIRS nighttime, cloud-clear OLR spectrum and 293K Planck distribution, [b] 650-680  $\text{cm}^{-1}$  subset, [c] HITRAN2016 spectral absorbance lines for CO<sub>2</sub> (Gordon et al., 2017). Note the excellent coincidence between AIRS detected radiance peaks and HITRAN CO<sub>2</sub> absorbance lines.

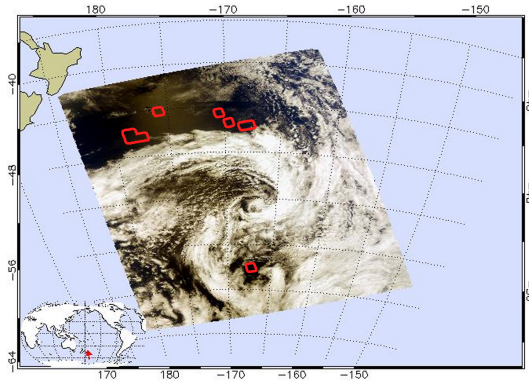


**Figure 3.** Visible image from granule 015 collected on January 1, 2016. Cloud-clear regions identified by the algorithm outlined in red.

42      uct, only naturally cloud-clear radiances with no mathematical adjustments contribute  
 43      to this analysis. Figure 3 provides a cloud-clear selection example rendered from the sun-  
 44      lit side of Earth to permit comparison with a visible image, however no daytime OLR  
 45      measurements contributed to this analysis. It is evident that the cloud detection algo-  
 46      rithm is conservative: visibly cloud-clear areas were not included and no visibly cloud-  
 47      contaminated areas were inadvertently included (in this example the cloud detection al-  
 48      gorithm has false positives but no false negatives).

49      Solar longwave infrared radiation reflected by clouds or Earth’s surface will com-  
 50      bine with terrestrial OLR, contaminating daytime measurements. To eliminate this source  
 51      of error, only nighttime measurements were utilized. When the AIRS solar zenith an-  
 52      gle (SZA) is  $<90^\circ$  AIRS observes the sunlit side of Earth, when  $90^\circ < \text{SZA} < 108^\circ$  it ob-  
 53      serves the twilight region and when  $\text{SZA} \geq 108^\circ$  it observes the nighttime region. Only  
 54      measurements at  $\text{SZA} \geq 108^\circ$  were utilized.

55      The AIRS mirror scans  $\pm 49.5^\circ$  from nadir and higher scan angles observe IR emis-  
 56      sion from higher in the atmosphere. Radiances from scan swath edges are signif-  
 57      icantly warmer or colder than nadir observations in the bands of radiatively-active gasses.  
 58      To reduce the effects of this anisotropy, only radiances at scan angles  $\leq 25^\circ$  were utilized.

59      The 2,378 individual channels comprising the AIRS IR sensor are monitored for  
 60      quality and flags are raised (0-2) whenever any should degrade. Measurements with qual-  
 61      ity value 0 “highest quality” and 1 “useful for scientific measurement” were utilized, while  
 62      quality value 2 “do not use” were excluded. Radiance measurements flagged as dust-contaminated  
 63      were similarly excluded, though these were rare ( $<0.01\%$ ).

## 64      2 Method

65      All AIRS radiance measurements meeting the selection criteria were analyzed in  
 66      this study (not a subset). Radiances for a given wavenumber channel were binned by month,  
 67      sub-binned in  $10^\circ$  latitude increments, then averaged. For example, 4,554 nighttime, cloud-  
 68      clear radiances at  $650.814 \text{ cm}^{-1}$  measured between  $0^\circ$  and  $10^\circ\text{N}$  contribute to the aver-  
 69      age radiance for January 2013 (figure 4, inset). 28.8% of sub-bins contain no data due  
 70      to heavy clouds, lack of nighttime measurements (e.g., polar summers) or failed detec-  
 71      tor channels. An additional 1.2% of all sub-bins containing fewer than 25 radiances meet-  
 72      ing the selection criteria were excluded to prevent trend skew by only a few measurements.  
 73      The median number of radiance measurements contributing to a monthly average for a  
 74      given channel in a given latitude bin is 5,064. Over time, some channel detectors suc-

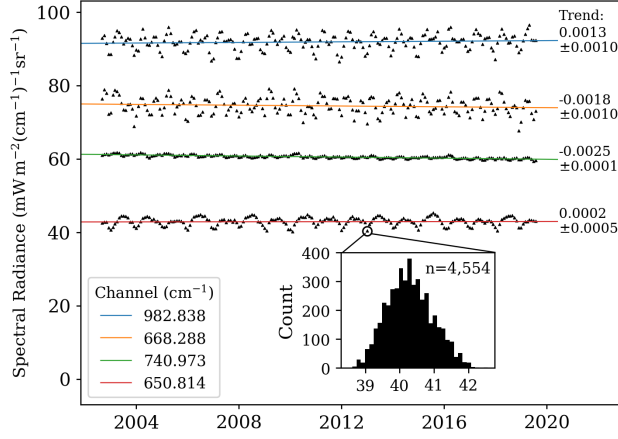


**Figure 4.** Least-squares regression fit to average monthly radiances for four AIRS channels in  $0^{\circ}$ - $10^{\circ}$  latitude bin. Remaining channels in all latitude bins were fit similarly.

75 cumb to solar radiation exposure and cease useful data production. Of the maximum  
 76 potential 17 year record, channels with fewer than five years were excluded for insuffi-  
 77 cient record length.

78 A straight line was fit by least-squares regression to the time series of monthly ra-  
 79 diance averages for each channel in each latitude bin. Seasonal temperature cycling was  
 80 eliminated as a source of trend bias by utilizing only complete years of measurement data  
 81 starting on 1 September 2002 and ending on 31 August 2019. An example line fitting  
 82 is provided in figure 4. The slope of each line is the spectral radiance trend  $\dot{L}_{\tilde{\nu}}$  ( $\text{mW m}^{-2}(\text{cm}^{-1})^{-1}\text{sr}^{-1}\text{yr}^{-1}$ )  
 83 and the uncertainty is  $\pm 1\sigma$ . Lines were fit to all channels in all 18 latitude bins.

### 84 3 Results: CO<sub>2</sub> Radiative Forcing

85 Reductions in OLR at  $650$ - $756 \text{ cm}^{-1}$  are presumed the result of rising atmospheric  
 86 CO<sub>2</sub> concentration. The reductions at detectable portions of the CO<sub>2</sub> P, Q, and R-branches  
 87 ( $650$ - $682 \text{ cm}^{-1}$ ) are minor compared to  $687$ - $756 \text{ cm}^{-1}$  where the majority of detectable  
 88 OLR reduction coincides with one of the CO<sub>2</sub> wings. OLR flux density change  $\delta E$  ( $\text{Wm}^{-2}$ )  
 89 was produced by integrating the spectral radiance trend  $\dot{L}_{\tilde{\nu}}$  over the range of CO<sub>2</sub>-affected  
 90 wavenumbers, then multiplying by 17 years and by  $\pi \text{ sr}$ , regarding the atmosphere as a  
 91 Lambertian emitter at these optically-thick channels:

$$92 \quad \delta E_{PQR} = 17\pi \int_{649.6\text{cm}^{-1}}^{682.0\text{cm}^{-1}} \dot{L}_{\tilde{\nu}} d\tilde{\nu} = -0.031 \pm 0.014 \text{ Wm}^{-2} \quad (1)$$

$$93 \quad \delta E_{wing} = 17\pi \int_{687.6\text{cm}^{-1}}^{756.3\text{cm}^{-1}} \dot{L}_{\tilde{\nu}} d\tilde{\nu} = -0.164 \pm 0.033 \text{ Wm}^{-2} \quad (2)$$

95 Integrals are depicted in the figure 6 inset, shaded regions. The majority of detectable  
 96 flux density change is attributable to the increasing wing absorption at  $687$ - $756 \text{ cm}^{-1}$ .  
 97 The symmetrical wing at  $580$ - $650 \text{ cm}^{-1}$  is outside of AIRS measurement range (see fig-  
 98 ure 7). Consequently, (1) + (2) is only a partial measurement of  $\delta E$  caused by rising  
 99 CO<sub>2</sub> and  $\delta E_{total}$  must be estimated. The P-branch and R-branch absorption lines flank-  
 100 ing the Q-branch are nearly symmetrical and rising CO<sub>2</sub> caused nearly-identical reduc-  
 101 tions in radiance. By extension, it is a reasonable prediction that the unmeasured  $580$ -  
 102  $650 \text{ cm}^{-1}$  wing has undergone OLR reduction by an amount similar to the measured  $687$ -  
 103  $756 \text{ cm}^{-1}$  wing. Therefore, total OLR flux density reduction due to rising CO<sub>2</sub> is esti-

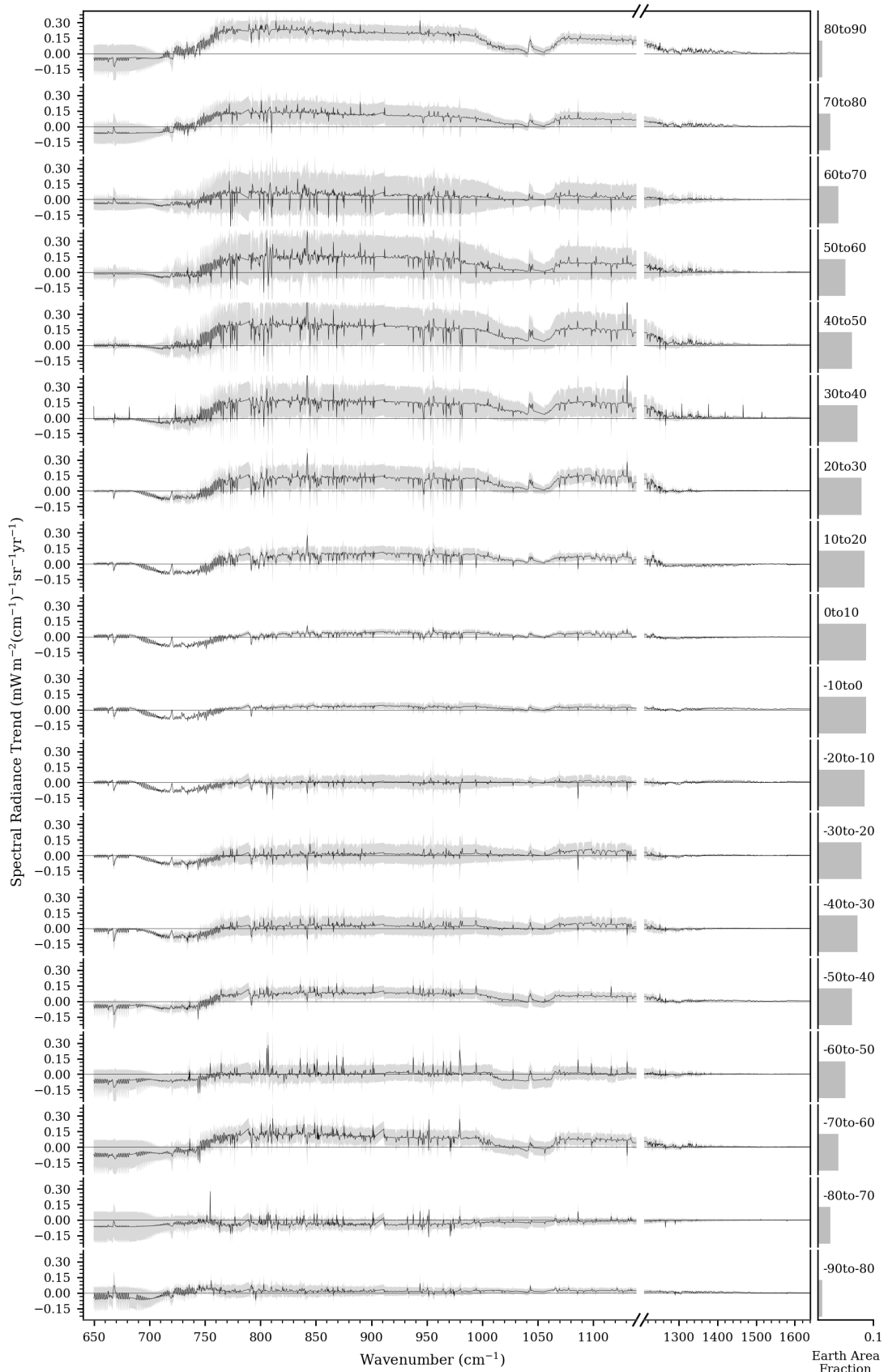


**Figure 5.** Nighttime, cloud-clear spectral radiance trend 2002-2019 in  $10^\circ$  latitude increments.  $\pm 1\sigma$  shaded.

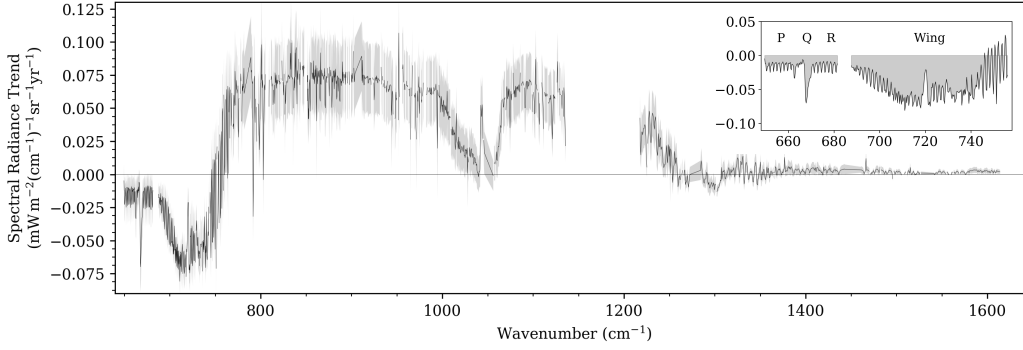


**Figure 6.** Global composite nighttime, cloud-clear spectral radiance trend 2002-2019.  $\pm 1\sigma$  shaded. Inset illustrates the integrals assessed to determine OLR reduction attributable to rising  $\text{CO}_2$ .

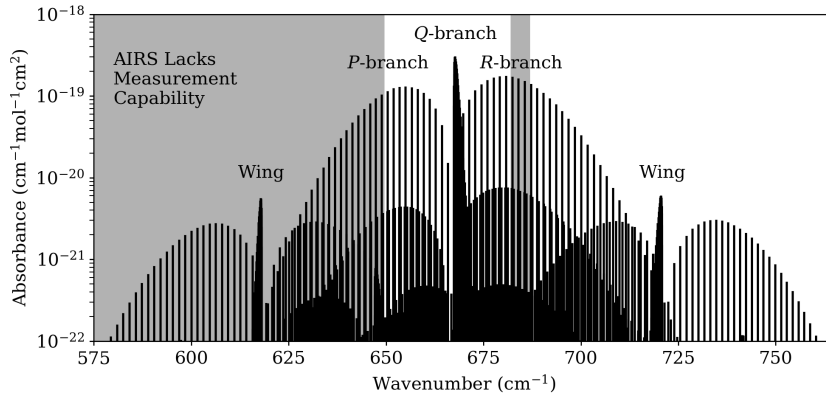


**Figure 7.** HITRAN2016  $\text{CO}_2$   $v_2$  absorption lines and AIRS measurement ranges

104 mated as:

$$105 \quad \delta E_{total} = \delta E_{PQR} + 2\delta E_{wing} = -0.358 \pm 0.067 \text{ W m}^{-2} \quad (3)$$

106 The computed flux density change, with reversed sign, is termed *radiative forcing* (RF).  
 107 It is reasonable to view (1) + (2) as a partial global measurement of nighttime, cloud-  
 108 clear  $\text{CO}_2$  RF and (3) as an empirically-derived estimation of total nighttime, cloud-clear  
 109  $\text{CO}_2$  RF added between 2002-2019.

110 Measurement of the atmospheric  $\text{CO}_2$  concentration increase that produced this  
 111 additional forcing was supplied by the NOAA ESRL's global monitoring division (Dlugokencky  
 112 & Tans, 2019). The combination of empirical measurement of TOA RF and  $\text{CO}_2$  con-  
 113 centration change permits a direct comparison to the climate model predictions of  $\text{CO}_2$ -  
 114 induced effective radiative forcing (ERF) taken from the IPCC's Fifth Assessment Re-  
 115 port (Stocker et al., 2013), also known as AR5. ERFs for 2000-2020 (368.9-412.1 ppm  
 116  $\text{CO}_2$ ) were interpolated for 2002-2019 (373.1-410.5 ppm  $\text{CO}_2$ ) and compared to AIRS  
 117 measurements in table 1.

118 AR5 ERFs were computed while holding surface temperature constant, a condi-  
 119 tion that does not hold for Earth. Therefore, an additional comparison was sought to  
 120 AIRS measurements of locations where surface/lower tropospheric temperatures did not  
 121 significantly change. Window wavenumber trends in Figure 5 indicate this is largely true

122 for 10°N-40°S and the area-weighted average forcing for this latitude range was included  
 123 in table 1. In either case, AR5 climate models appear to over-predict CO<sub>2</sub> RF.

**Table 1.** Radiative Forcing from +37 ppm CO<sub>2</sub>

Source	CO <sub>2</sub> RF, $-\delta E_{total} \pm 1\sigma$
AIRS 90°N-90°S	$0.358 \pm 0.067 \text{ Wm}^{-2}$
AIRS 10°N-40°S	$0.434 \pm 0.047 \text{ Wm}^{-2}$
IPCC AR5 ERF	$0.508 \pm 0.102 \text{ Wm}^{-2}$

#### 124 4 Sources of Error

125 Radiance and flux density changes in the CO<sub>2</sub>  $v_3$  band (2300-2380 cm<sup>-1</sup>) were not  
 126 characterized since less than 0.01% of the Earth's infrared radiant exitance occurs in this  
 127 band.

128 The AIRS instrument measurement gap at 681.993-687.601 cm<sup>-1</sup> prevents trend  
 129 quantification in a narrow portion of the  $v_2$  R-branch. Interpolation from adjacent chan-  
 130 nels yields 0.0038 Wm<sup>-2</sup> of forcing was not measured, causing underestimate of  $\delta E_{total}$   
 131 by 1.2%.

132 The unmeasured 580-650 cm<sup>-1</sup> wing was assumed to undergo radiance reduction  
 133 identical to the measured wing, however, the 580-650 cm<sup>-1</sup> wing overlaps with stronger  
 134 water vapor absorption lines. The assumption of symmetry is conservatively high and  
 135 actual OLR reductions at 580-650 cm<sup>-1</sup> are expected to be lower than at 687-756 cm<sup>-1</sup>.  
 136 Trend asymmetry between the two wings was observed in DLR reported by Feldman et  
 137 al. (2015): the 580-650 cm<sup>-1</sup> wing showed less forcing change over time relative to the  
 138 687-756 cm<sup>-1</sup> wing, particularly in the southern great plains where atmospheric mois-  
 139 ture content is higher.

140 Over 17 years, detector stability is more important than absolute accuracy as un-  
 141 biased noise does not preclude long-term trend analysis. One possible cause of trend bias  
 142 is gradual accumulation of molecular contaminants on the AIRS detector mirror. A hy-  
 143 pothetical 100Å contamination layer is predicted by H. Aumann et al. (2000) to increase  
 144 the mirror emissivity variation by 0.001, producing cold scene brightness temperatures  
 145 at 650-800 cm<sup>-1</sup> that are 0.1-0.2° K warmer than reality. If such a contamination layer  
 146 were gradually building up during the observation period, warming trends could be am-  
 147 plified and cooling trends (including forcing) could be diminished. Evidence of mirror  
 148 contamination between 2002-2010 has been reported by others (H. H. Aumann et al.,  
 149 2018) to affect AIRS midwave IR channels (2181-2665 cm<sup>-1</sup>) which were not utilized in  
 150 this study.

151 This analysis assumed isotropic atmospheric emissions despite radiances from scan  
 152 swath edges measuring significantly warmer or colder than nadir observations. Over time,  
 153 if proportionally more (or fewer) swath edge measurements meet the quality and cloud-  
 154 clear selection criteria, trend bias will result. As a check, trend fits and integrals were  
 155 recomputed with a wider and narrower scan angle ranges, including and excluding larger  
 156 portions of scan swath edges. Fewer total measurements contribute to a restricted scan  
 157 angle analysis with a commensurate increase in uncertainty. Results in table 2 indicate  
 158 that including scan swath edges causes overestimation of forcing:  $\delta E_{total}$  produced from  
 159  $\pm 25^\circ$  and  $\pm 49.5^\circ$  measurements are 3.8% and 10.4% higher than from  $\pm 12.5^\circ$  measure-  
 160 ments, respectively.

**Table 2.** Swath Edge Radiance Impact

Scan Angle	Radiances at 650-756 $\text{cm}^{-1}$ (count)	$\text{CO}_2$ Forcing $-\delta E_{total} \pm 1\sigma (\text{Wm}^{-2})$
$\pm 49.5^\circ$	$25.7 \times 10^9$	$0.381 \pm 0.067$
$\pm 25.0^\circ$	$15.5 \times 10^9$	$0.358 \pm 0.067$
$\pm 12.5^\circ$	$7.8 \times 10^9$	$0.345 \pm 0.068$

## 161 5 Conclusion

162 Seventeen years of AIRS nighttime, cloud-clear OLR measurements reveal  $0.358 \pm 0.067$   
 163  $\text{Wm}^{-2}$  additional radiative forcing induced by +37 ppm atmospheric  $\text{CO}_2$ . Unfortunately,  
 164 AIRS lacks measurement capability at 580-650  $\text{cm}^{-1}$  for complete  $\text{CO}_2$   $\nu_2$  band char-  
 165 acterization, therefore this empirical estimate of increased forcing was devised by pre-  
 166 suming  $\text{CO}_2$   $\nu_2$  wing symmetry and doubling the observed wing's radiative forcing. The  
 167 IPCC Fifth Assessment Report predicted  $0.508 \pm 0.102 \text{ Wm}^{-2}$  RF resulting from this  $\text{CO}_2$   
 168 increase, 42% more forcing than actually observed. The lack of quantitative long-term  
 169 global OLR studies may be permitting inaccuracies to persist in general circulation model  
 170 forecasts of the effects of rising  $\text{CO}_2$  or other greenhouse gasses.

## 171 Acknowledgments

172 The author acknowledges Robert Amour and Leon de Almeida for analysis program cre-  
 173 ation, Nolan Nicholson for the custom data plotting program and Steven J. Martin for  
 174 the many informative conversations. All data is available at [link].

## 175 References

- 176 Aumann, H., Gregorich, D., Gaiser, S., Hagan, D., Pagano, T., Strow, L., & Ting,  
 177 D. (2000). Airs algorithm theoretical basis document. *Level 1B, Part, 1*, 70.
- 178 Aumann, H. H., Manning, E. M., & Broberg, S. (2018). Radiometric stability in 16  
 179 years of airs hyperspectral infrared data. In (Vol. 10764, p. 1076400).
- 180 Dlugokencky, E., & Tans, P. (2019). *Noaa/esrl*. [www.esrl.noaa.gov/gmd/ccgg/  
 181 trends/](http://www.esrl.noaa.gov/gmd/ccgg/trends/). (Accessed 11-2019)
- 182 Feldman, D. R., Collins, W. D., Gero, P. J., Torn, M. S., Mlawer, E. J., & Shippert,  
 183 T. R. (2015). Observational determination of surface radiative forcing by  $\text{CO}_2$   
 184 from 2000 to 2010. *Nature*, *519*(7543), 339.
- 185 Gordon, I. E., Rothman, L. S., Hill, C., Kochanov, R. V., Tan, Y., Bernath, P. F.,  
 186 ... others (2017). The hitran2016 molecular spectroscopic database. *Journal  
 187 of Quantitative Spectroscopy and Radiative Transfer*, *203*, 3–69.
- 188 Harries, J. E., Brindley, H. E., Sagoo, P. J., & Bantges, R. J. (2001). Increases in  
 189 greenhouse forcing inferred from the outgoing longwave radiation spectra of  
 190 the earth in 1970 and 1997. *Nature*, *410*(6826), 355.
- 191 Stocker, T. F., Qin, D., Plattner, G.-K., Tignor, M., Allen, S. K., Boschung, J., ...  
 192 others (2013). Climate change 2013: The physical science basis.
- 193 Teixeira, A. S. T. (2013). *Airs/aqua l2 cloud-cleared infrared radiances (airs-only)  
 194 v006*. <https://doi.org/10.5067/Aqua/AIRS/DATA205>. (Accessed 10-2019)